Applied Physics Letters

Dynamic multiple nanoparticle trapping using metamaterial plasmonic tweezers

Cite as: Appl. Phys. Lett. **118**, 021107 (2021); https://doi.org/10.1063/5.0032846
Submitted: 11 October 2020 . Accepted: 18 December 2020 . Published Online: 12 January 2021

Domna G. Kotsifaki, Viet Giang Truong, and Síle Nic Chormaic

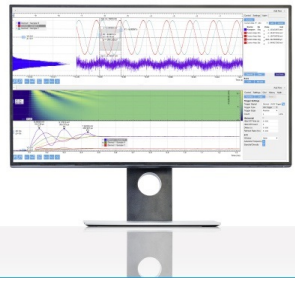

Applied Physics Letters ARTICLE scitation.org/journal/apl

Dynamic multiple nanoparticle trapping using metamaterial plasmonic tweezers

Cite as: Appl. Phys. Lett. **118**, 021107 (2021); doi: 10.1063/5.0032846
Submitted: 11 October 2020 · Accepted: 18 December 2020 ·
Published Online: 12 January 2021

Domna G. Kotsifaki, Viet Giang Truong,[a] and Síle Nic Chormaic

AFFILIATIONS

Light-Matter Interactions for Quantum Technologies Unit, Okinawa Institute of Science and Technology Graduate University, Onna, Okinawa 904-0495, Japan

[a]Author to whom correspondence should be addressed: v.g.truong@oist.jp

ABSTRACT

Optical manipulation has attracted remarkable interest owing to its versatile and noninvasive nature. However, conventional optical trapping remains inefficient in the nanoscopic world. The emergence of plasmonics in recent years has brought a revolutionary change in overcoming limitations due to diffraction and the requirements for high trapping laser powers. Among the near-field optical trapping cavity-based systems, Fano-resonant optical tweezers have a robust trapping capability. In this work, we experimentally demonstrate sequential trapping of 20 nm particles through the use of metamaterial plasmonic optical tweezers. We investigate the multiple trapping via trap stiffness measurements for various trapping configurations at low and high incident laser intensities. Our plasmonic configuration could be used as a light-driven nanoscale sorting device under low laser excitation. Our results provide an alternative approach to trap multiple nanoparticles at distinct hotspots, enabling ways to control mass transport on the nanoscale.

Light interactions with metallic nanostructures demonstrate unique properties, which have drawn the attention of researchers, giving rise to an emergent field called plasmonics. Currently, the study of artificial metallic nanostructures[1] has greatly expanded the range of electromagnetic properties exhibited by naturally occurring materials. Because metamaterials are produced by structuring their unit elements on a spatial scale that is smaller than the light wavelength, they occupy a unique niche between photonic crystals and regular materials. Numerous applications of metamaterials include superlenses,[2] spintronics,[3] cloaking,[4] and lasing spasers.[5] A state-of-the-art design, which presents a resonant magnetic response, is the asymmetric split-ring resonator (ASR).[6–8] In this structure, both the radiant and subradiant modes are supported due to the structural symmetric breaking and the interference between these two modes generates a Fano resonance peak.[1] Fano-resonant metamaterials enable strong selective enhancement of the electromagnetic fields in their immediate vicinity, thereby considerably boosting the interaction of light with matter placed in close proximity to the meta-molecule. Hence, even with a weak perturbation in the electromagnetic environment of the metamaterial, the scattering properties can be significantly altered.[9] Owing to their physical properties, Fano-resonant nanosystems can enhance the performance for nanophotonic applications such as Raman spectroscopy for molecular detection[10,11] and optical trapping.[8]

Optical tweezers[12,13] are an attractive technique for the direct manipulation of particles in a free-solution environment. Benefiting from the rapid development of localized surface plasmon technology, plasmonic optical trapping can break the optical diffraction limit and further enhances the near electromagnetic field, leading to strong optical gradient forces.[14] As a result, plasmonic optical tweezers (POTs),[15,16] have led to numerous fundamental studies and technical applications. For example, double nano-aperture-assisted POTs have been applied to proteins and other biomolecules,[17] providing a way to better understand their interactions in real time. While much previous work has studied single-particle trapping, the trapping of multiple particles has attracted great interest with applications in physics and biology.[18,19] Furthermore, by arraying the metallic features in nanostructures,[8,18,20–23] many trapping sites can be activated at the same time, permitting simultaneous analysis of several nanoparticles, locally trapped at well-defined positions of the plasmonic devices. The ability to trap multiple particles in periodic arrays suggests the possibility of creating synthetic nanomaterials[20,24,25] and may enable on-chip biological trapping and analysis. For example, sequential optical trapping of a single 30 nm particle has been demonstrated using a double

nanoaperture array with 44 nm connecting nanoslots.[18] The authors achieved sequential trapping of single nanoparticles using an on-resonance laser with an intensity of 0.51 mW/μm^2.[18] Recently, we demonstrated 20 nm polystyrene (PS) nanoparticle trapping on an array of asymmetrical split-ring (ASR) nanoapertures.[8] A relatively large normalized trap stiffness of 8.65 fN/nm at the near-resonant condition was achieved for a trapping laser intensity of 1.0 mW/μm^2.[8] This high trap stiffness enabled trapping at low incident intensities and leads to a variety of potential applications in chemistry and biosensing.

In this paper, we use Fano-resonant metamaterial optical tweezers to tightly trap 20 nm polystyrene (PS) particles in succession. We perform trap stiffness measurements at several plasmonic hotspots and trapping wavelengths. We show that a trapped nanoparticle is transferred toward the plasmonic nanostructure and to a plasmonic hotspot, which is not necessarily that which provides the strongest optical forces. By switching off and on the trapping laser beam, the trapped particle moves to the adjacent trapping position due to its Brownian motion. This implies that our plasmonic configuration may operate as a plasmonic sorting device. We show that the experimental trap stiffness and the theoretical optical force curves vs trapping wavelength, for each trapping position configuration, follow a similar trend, indicating the dominance of the Fano-resonant mechanism in the trapping performance at laser intensities up to 1.10 mW/μm^2. By multiple particle trapping without forming any clusters, we foresee that our plasmonic device will open up avenues for nanoparticle manipulation in a lab-on-chip environment. In the context of drug design, it may enable a noninvasive study of biomolecular interactions or evaluation of the binding forces between DNA–ligands.[17]

For the optical trapping measurements, we used a custom-built trapping setup, with a tunable, continuous-wave Ti:sapphire laser (Coherent-MBR-110) as the trapping laser [Fig. 1(a)]. The laser beam was expanded to overfill a high-numerical aperture oil-immersion microscope objective lens (NA = 1.25, 100×) and was focused near the metamaterial. Dielectric PS particles of 20 nm diameter were

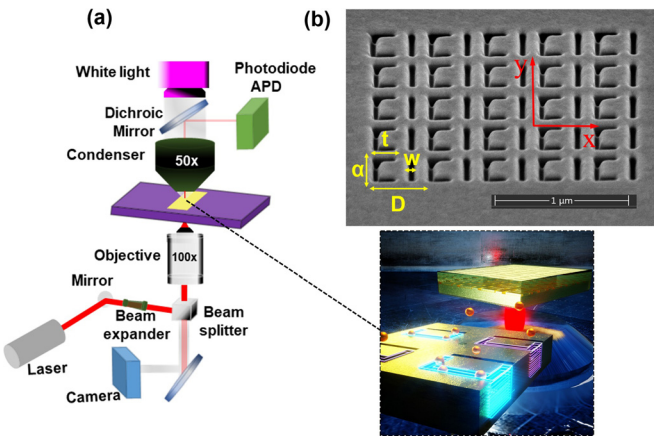

FIG. 1. (a) Schematic illustration of the experimental setup, showing a zoomed-in image of the trap substrate region. (b) Scanning electron microscope (SEM) image, viewed at 52° from the surface normal of the metamaterial. The geometrical dimensions of each metamolecule unit are $D = 405 \pm 2$ nm, vertical slit $\alpha = 310 \pm 4$ nm, horizontal slit $t = 164 \pm 3$ nm, and slit width $w = 44 \pm 2$ nm.

diluted into heavy water with a volume concentration of 0.0625%. A small amount of surfactant Tween-20 with a volume concentration of 0.1% was added to the particle solution, and the final solution was sonicated to further prevent the formation of aggregates. To detect a trapping event, the transmitted laser light was collected through a 50× objective lens and sent to an avalanche photodiode (APD). We monitored the APD signal using a 100 kHz sampling rate data acquisition card. We fabricated the metamaterial structure using focused ion beam (FIB) milling through a 50-nm gold thin film. Figure 1(b) shows a scanning electron microscope (SEM) image of an array of 5×5 metamolecules with a periodicity along both x and y of 405 nm. The metamaterial used for the trapping experiments consisted of an array of 17 (x-direction) and 15 (y-directions) ASR metamolecules. From the transmission and reflection spectra of the metamaterial, which were measured using a microspectrophotometer (MCRAIC 20/30PV), we calculated the absorption spectrum to determine the Fano resonance peak at 928 nm.[8]

To gain insight into the physical mechanism underlying the trapping of nanoparticles in specific trapping configurations, we performed finite element method simulations using the COMSOL Multiphysics software package. The geometric parameters used in the simulations were those obtained from SEM images [Fig. 1(b)]. We calculated the near-field (E-field) distribution, the optical forces, and the potentials when the metamolecule unit was polarized along the x-direction [Fig. 1(b)]. The optical forces on the trapped nanoparticle were calculated based on time-averaged Maxwell's Stress Tensor method.[26,27] We assumed that a 20 nm PS nanoparticle was positioned in the strongest near-field intensity region on the water side of the open nanoaperture area where the equilibrium position exists. Potentials were calculated by integrating the optical forces along the z-axis.

Figure 2(a) shows the simulated enhancement of the electric field distribution on the xy-plane for a resonant wavelength of 965 nm. When the ASR unit is illuminated by light, the strong light–matter coupling creates three plasmonic configurations, as shown by the noted regions of Fig. 2(a). The theoretical Fano resonance peak appears at 965 nm. It is associated with excitation of circulating currents oscillating in the two types of nanoapertures, that is, the C-type and l-type. Such asymmetric modes yield magnetic dipole moments oriented normal to the array plane, oscillating synchronously in all metamolecules.[28,29] Figure 2(b) shows the theoretical optical force exerted on a 20 nm PS particle for the three possible trapping configurations as a function of the incident trapping wavelength. Figures 2(c) and 2(d) show the trapping potentials for off- and on-resonance conditions, respectively. From Fig. 2(b), the nanoparticle appears to prefer to be trapped at the position where the near field exerts a maximum force upon it [trapping Configuration 1, Fig. 2(a)]. Moreover, the geometry of our device means that the nanoparticle can also be trapped at positions where the optical force is less strong compared to Configuration 1 [Figs. 2(a)–2(c)]. Furthermore, we observe a redshift of the optical force in trapping Configuration 1 compared to trapping Configurations 2 and 3. This redshift originates from the Fano resonance contributions of each individual hotspot.[8] For x-polarized excitation, the antisymmetric mode, which is associated with the absorption resonance, can dominate compared to the usual symmetric one. As a consequence, the strength of the induced currents can reach high values in trapping Configuration 1 compared to Configurations 2

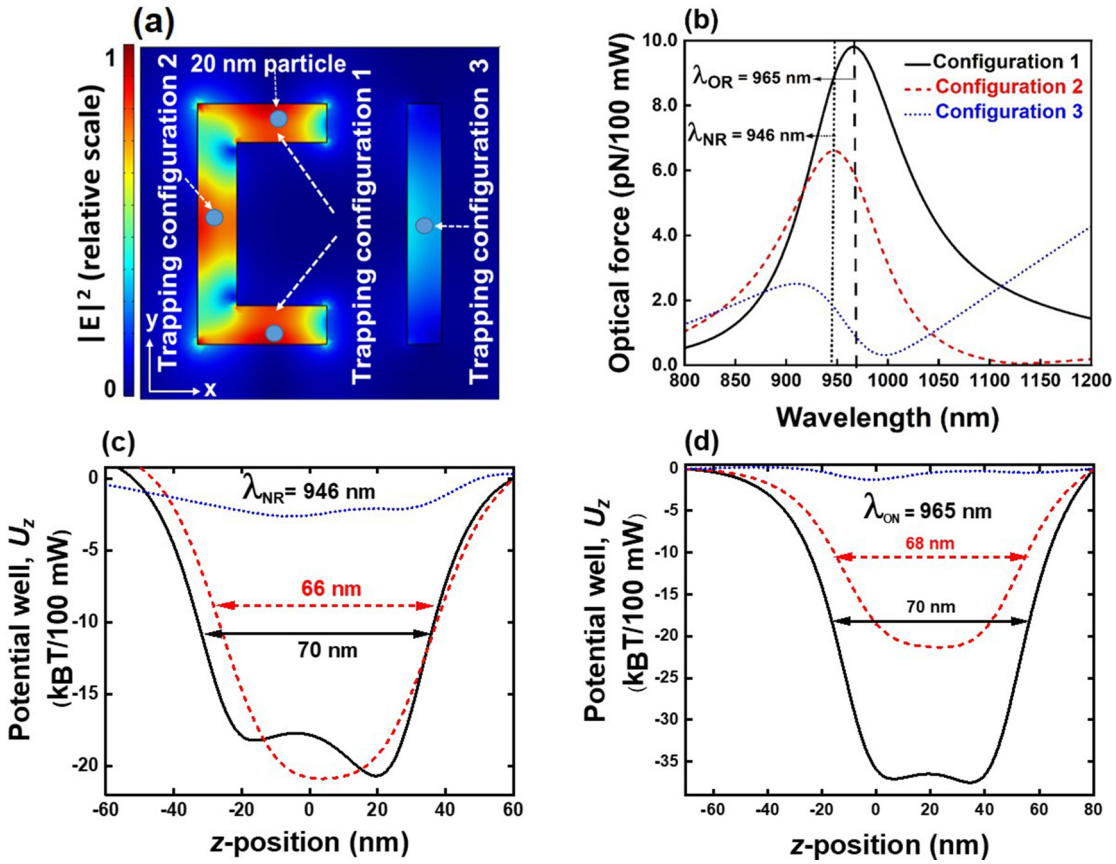

FIG. 2. (a) Near-field (*E*-field) distribution of an ASR unit at a simulated resonance of 965 nm for the *x*-direction. The three possible trapping configurations are indicated, where trapping Configuration 1 consists of two locations on the ASR metamolecule. (b) The optical forces exerted on a 20 nm PS particle in the three trapping configurations. Potential well, U_z, for each trapping position along the *z*-axis for (c) off-resonance illumination at 946 nm and (d) on-resonance conditions at 965 nm. In our model, the plane at $z = 0$ is the boundary between the gold (Au) film and the SiO_2 interface. The nanoaperture pattern was cut into the glass substrate to a depth of 20 nm to provide a short distance over which the nanoparticle can move close to the gold/glass interface.

and 3, thereby leading to the redshift. We determine the full-width-at-half-maximum (FWHM) of the trapping wells in the *z*-direction for each trapping position when on resonance [Fig. 2(d)], and we calculate the respective theoretical trap stiffnesses to be $\kappa_1 = 4.16$ fN/nm, $\kappa_2 = 1.16$ fN/nm, and $\kappa_3 = 0.28$ fN/nm.

Figure 3(a) shows a trace of a typical transmission signal recorded on the APD as a function of time through an array of ASR metamaterials in a solution of 20 nm PS beads. After observing up to five trapping events, we block the trapping laser beam for up to 20 s and then repeat the experimental run. This process is repeated four times, yielding a total of four runs per experiment, which shows the repeatability of trapping events. Note that Fig. 3(a) shows only two such runs for a single experiment. The four-run limit is due to heating of the metamaterial. We then repeat each experiment (of four runs) four times, yielding a total of 16 experimental runs. We wait for 15 min between each experiment to allow for complete heat dissipation.

Zoomed-in images of Fig. 3(a) reveal multiple step-like jumps, typically within 4 s, indicating trapping events [see Fig. 3(b)]. At 65 s, the trapping laser is turned on and the first PS nanoparticle is trapped after two seconds (67 s). After one more second (68 s), several nanoparticles are sequentially trapped at plasmonic hotspots of the metamaterial device. We observe five distinct steps, relative to the vacant level, of the sequential nanoparticle trapping. The distance between closest neighbor hotspots is 155 nm. The FWHM of the trapping potential well is approximately 70 nm for each trapping position. This is narrower than the distance between the hotspots. Therefore, we assume that the nanoparticle is stably trapped at a given hotspot for a long period of time during which the trapping laser is on, preventing its transportation to any neighboring hotspot under illumination.

To investigate multiple trapping using the Fano-resonant metamaterial plasmonic tweezers, we measured the trap stiffness for each trapping event, in several trapping configurations, for low (0.55 mW/μm^2) and high (1.10 mW/μm^2) incident laser intensities. The overdamped Langevin equation[30] can be used to describe the particle motion within the trap,

$$\frac{dx(t)}{dt} = \frac{\kappa_{tot}}{\gamma}x(t) + \left(\frac{2k_BT}{\gamma}\right)^{1/2}\zeta(t), \quad (1)$$

where γ is the viscous damping, $x(t)$ is the displacement of the particle from the equilibrium point, κ_{tot} is the total trap stiffness, $\zeta(t)$ is the

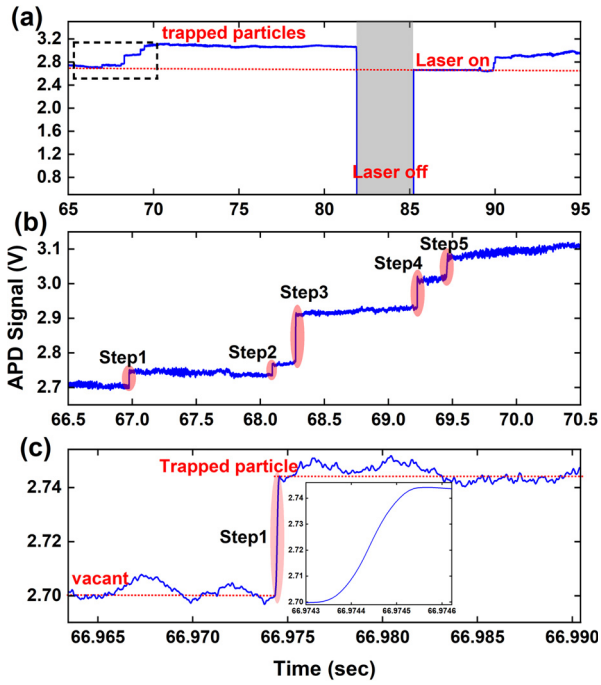

FIG. 3. (a) Laser transmission through the ASR array, showing plasmonic trapping events for 20 nm PS particles recorded over 30 s during two experimental runs. The incident laser intensity is 0.53 mW/μm^2 at the sample plane, and the trapping wavelength is 923 nm. (b) Expanded view of several trapping events of the black dashed rectangular box in (a). (c) The expanded time trace of the first trapping event in (b), representing a time interval of 0.3 ms.

white noise, k_B is the Boltzmann constant, and T is the temperature. Using an exponential fit of the trapping region, the trap stiffness is determined using the following equation:[30]

$$\tau = \frac{\gamma}{\kappa_{tot}}, \tag{2}$$

where τ is the exponential decay time. We consider the Stoke drag coefficient and adjust it with the Faxen correction factor.[18,30]

Figure 4 shows the values of the trap stiffness calculated for each trapping event for four trapping runs (turning on and off the trapping beam) averaged over four experiments. A near-resonance trap wavelength of 930 nm and laser intensities of [Fig. 4(a)] 0.55 mW/μm^2 and [Fig. 4(b)] 1.10 mW/μm^2 were used. In total, 256 trapping events were analyzed (four experiments per day, four runs per experiment, and four trapping events per run) for each value of the laser intensity. The trap stiffness per trapping event per run is averaged over the four experiments.

To confirm single nanoparticle trapping, we analyzed data for comparable step heights [see Fig. 3(b)] for each observable trapping event. Since the transportation of the nanoparticle due to Brownian motion is inherently very slow when the trapping laser is off, only particles close to the excited plasmonic hotspot can be immobilized into plasmonic hotspots.[31] We note that the nanoparticle that is closest to any one of the plasmonic hotspots of the ASR unit [Fig. 2(a)] will be trapped at this specific hotspot under the influence of optical forces. We define two possible trapping configurations based on the theoretical values of the trap stiffnesses. The experimental values of trap stiffness can then be roughly categorized into these two regions. In Fig. 4, the shaded regions are given as guides to the eye and are centered around the theoretical values. It should be noted that a 20% deviation of the actual particle's size was taken into account in the trap stiffness calculations.

Figures 5(a) and 5(b) show the trap stiffnesses for the two trapping configurations (Configurations 1 and 2 [Fig. 2(a)]) vs incident trapping wavelength for low (0.55 mW/μm^2) and high (1.10 mW/μm^2) incident laser intensities, respectively. The absorption spectrum is also plotted.[8] The maximum trap stiffness is achieved for a trapping wavelength near resonance for both trapping configurations. Unsurprisingly, the plasmonic hotspot with the weaker near field (Configuration 2) provides a smaller trap stiffness compared to the strong near-field hotspot (Configuration 1). Using Lorentz fitting of the experimental trap stiffness values, we determined the trap stiffness peak for each trapping position at 931 nm for low incident trapping

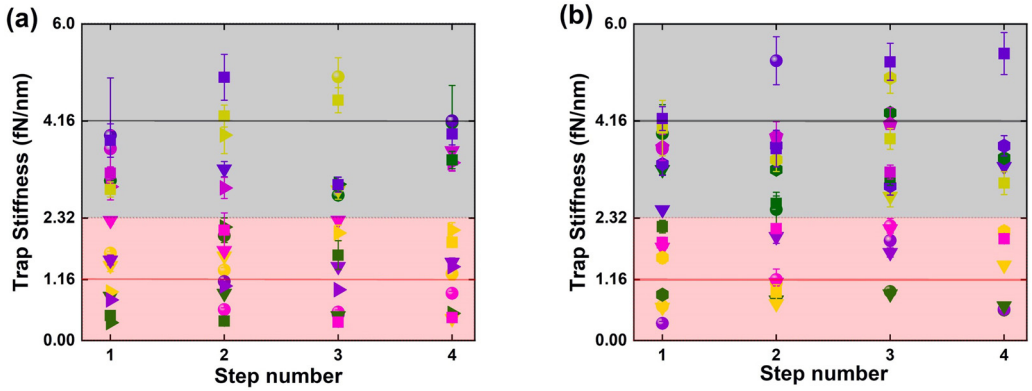

FIG. 4. Trap stiffness calculated for each trapping event (step number) for each of the four runs averaged over four experiments and shown for four days of experiments. Laser intensities are (a) 0.55 mW/μm^2 and (b) 1.10 mW/μm^2 near resonance at 930 nm. The horizontal lines at 4.16 fN/nm and 1.16 fN/nm indicate the theoretical values for Configurations 1 and 2 on the array [see Fig. 2(a)]. The shaded regions are given as guides to the eye only and are centered around the theoretical values. The y-error is the standard deviation of the trap stiffness measurements over four experiments. Symbols: run 1 (green), run 2 (yellow), run 3 (purple), run 4 (pink), day 1 (circle), day 2 (triangle), day 3 (diamond), and day 4 (square).

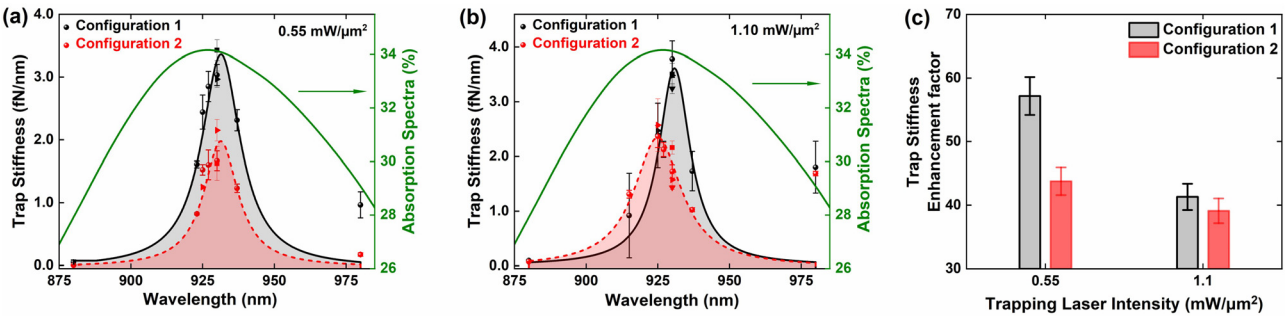

FIG. 5. Absorption spectra (green line) and trap stiffness vs trapping wavelength and trapping positions for laser intensities of (a) 0.55 mW/μm^2 and (b) 1.10 mW/μm^2. All red and black lines are Lorentz fitting results from the experimental data. The *y*-error is the standard deviation of the trap stiffness measurements. (c) Trap stiffness enhancement factor as a function of trapping positions for low and high laser intensities.

intensity, and the result is in agreement with our previous observations.[8] However, at a high (1.10 mW/μm^2) laser intensity, we observe a redshift of the trap stiffness resonance peak as the particle moves from the weaker [Configuration 2, Fig. 2(a)] to the stronger (Configuration 1) hotspot as shown in Fig. 5(b). This is in reasonable agreement with the theoretical optical force calculations [see Fig. 2(b)]. Moreover, we notice that the FWHM of the absorption spectra (green lines) is much broader than those for the trap stiffness curves for both low and high laser trapping intensities. This is in agreement with our previous observations.[8]

Figure 5(c) shows the trap stiffness enhancement factor vs laser intensities for both trapping configurations. The trap stiffness enhancement is determined by normalizing the trap stiffness at the Lorentz peak for each of the two trapping configurations to that obtained at 880 nm, a wavelength far from the resonance peak. The enhancement, which is due to the strong interaction between the trapped nanoparticle and the Fano resonance, decreases as the particle moves from trapping Configuration 1 to Configuration 2 for the higher laser intensity. Because the trap stiffness is directly proportional to the optical forces and to the near-field intensity, the trap stiffness enhancement factor follows the near-field strength of each plasmonic hotspot. The three trapping configurations of our ASR metamaterial can be used to qualitatively identify the nanoparticle's location by measuring the trap stiffness.

A common characteristic of all metallic nanostructures is absorption and Ohmic losses in the metal, leading to Joule heating of the surrounding environment.[32,33] Photo-induced heat generation in metallic nanowires was investigated by using a thermal microscopy technique.[32] The authors showed that the local distribution of the temperature in plasmonic nanostructures was fairly uniform despite the nonuniformity of the heat source density.[32] This feature induces mismatch between the thermal hotspots, which arise from the areas where charges can freely flow, and plasmonic hotspots from the tip effects and charge accumulation at the metal interface.[32] Additionally, the local temperature increase results in thermally induced fluid convection, which exerts drag forces on suspended nanoparticles in a liquid environment.[34,35] These convection flows have improved the delivery of nanoparticles toward plasmonic hotspots where they can be trapped.[34–36] Although the gradient forces exerted on a nanoparticle are strong in trapping Configuration 1 [see Fig. 2(b)], due to their short range, the nanoparticle tends to be trapped at the hotspot closest to it. We can determine the specific position at which the nanoparticle will be trapped using the trap stiffness calculations. This sorting performance stems from the tunability of the potential wells and has applications in the trapping and sorting of biomolecules. However, to further investigate the origin of this mechanism, an analytical theoretical heating model of the metamaterial nanostructure would be required to explore, in-depth, the contribution of thermally induced effects on the trapping performance and the particle's motion; this will be a focus of future work.

The fact that the trap stiffness of each plasmonic hotspot [Figs. 5(a) and 5(b)] follows a similar trend as the corresponding optical gradient force [Fig. 2(b)] confirms the strong contribution of the Fano resonance to the trapping efficiency, as shown in our previous work.[8] However, the collective heating of many hotspots, which lead to an increase in the local temperature, results in convection effects. These photo-induced thermal effects may influence the trap stiffness enhancement factor at high laser intensities, as shown in Fig. 5(c). A certain range of laser intensities exists over which thermal effects are in synergy with the near field, leading to strengthening of the optical trap. The above-mentioned analysis indicates the extraordinary trapping ability of our device to demonstrate sequential trapping of 20 nm particles at low and high laser intensities. The exact nature of this trapping ability depends on several parameters and must be addressed, but it is beyond the scope of this work.

It remains a formidable challenge to sort out subwavelength particles with single-nanometer precision. Here, we have experimentally demonstrated a platform based on a metamaterial consisting of an array of ASR units for multiple nanotrapping. We have studied the performance of our device by using trap stiffness measurements as a function of trapping configuration and trapping wavelength for both low and high laser intensities. We have shown that subwavelength, dielectric nanoparticles can be transported to the plasmonic system by turning on and off the trapping laser beam when at near resonance. By using multiple plasmonic traps on a metamaterial, controlled manipulation of nanoparticles and/or biomolecules for time periods lasting minutes in real time is feasible.

The authors would like to thank the Engineering Support Section at OIST for access to the nanofabrication facilities, Metin Ozer for technical assistance, Ella Maru Studio for one inset image, and OIST Editing Section for reviewing this manuscript.

This work was supported by funding from the Okinawa Institute of Science and Technology Graduate University. D.G.K. acknowledges support from JSPS Grant-in-Aid for Scientific Research (C) Grant No. GD1675001.

DATA AVAILABILITY

The data that support the findings of this study are available from the authors upon reasonable request.

REFERENCES

[1]B. Luk'yanchuk, N. I. Zheludev, S. A. Maier, N. J. Halas, P. Nordlander, H. Giessen, and T. C. Chong, "The Fano resonance in plasmonic nanostructures and metamaterials," Nat. Mater. **9**, 707 (2010).
[2]X. Zhang and Z. Liu, "Superlenses to overcome the diffraction limit," Nat. Mater. **7**, 435 (2008).
[3]G. Armelles, L. Bergamini, N. Zabala, F. García, M. L. Dotor, L. Torné, R. Alvaro, A. Griol, A. Martínez, J. Aizpurua, and A. Cebollada, "Metamaterial platforms for spintronic modulation of mid-infrared response under very weak magnetic field," ACS Photonics **5**, 3956 (2018).
[4]P. Alitalo and S. Tretyakov, "Electromagnetic cloaking with metamaterials," Mater. Today **12**, 22 (2009).
[5]N. I. Zheludev, S. L. Prosvirnin, N. Papasimakis, and V. A. Fedotov, "Lasing spaser," Nat. Photonics **2**, 351 (2008).
[6]V. A. Fedotov, M. Rose, S. L. Prosvirnin, N. Papasimakis, and N. I. Zheludev, "Sharp trapped-mode resonances in planar metamaterials with a broken structural symmetry," Phys. Rev. Lett. **99**, 147401 (2007).
[7]K. Tanaka, E. Plum, J. Y. Ou, T. Uchino, and N. I. Zheludev, "Multifold enhancement of quantum dot luminescence in plasmonic metamaterials," Phys. Rev. Lett. **105**, 227403 (2010).
[8]D. G. Kotsifaki, V. G. Truong, and S. Nic Chormaic, "Fano-resonant, asymmetric, metamaterial-assisted tweezers for single nanoparticle trapping," Nano Lett. **20**, 3388 (2020).
[9]F. Hao, P. Nordlander, Y. Sonnefraud, P. V. Dorpe, and S. A. Maier, "Tunability of subradiant dipolar and Fano-type plasmon resonances in metallic ring/disk cavities: Implications for nanoscale optical sensing," ACS Nano **3**, 643 (2009).
[10]F. Le, D. W. Brandl, Y. A. Urzhumov, H. Wang, J. Kundu, N. J. Halas, J. Aizpurua, and P. Nordlander, "Metallic nanoparticle arrays: A common substrate for both surface-enhanced Raman scattering and surface-enhanced infrared absorption," ACS Nano **2**, 707 (2008).
[11]C. Wu, A. B. Khanikaev, R. Adato, N. Arju, A. A. Yanik, H. Altug, and G. Shvets, "Fano-resonant asymmetric metamaterials for ultrasensitive spectroscopy and identification of molecular monolayers," Nat. Mater. **11**, 69 (2012).
[12]A. Ashkin, J. M. Dziedzic, J. E. Bjorkholm, and S. Chu, "Observation of a single-beam gradient force optical trap for dielectric particles," Opt. Lett. **11**, 288 (1986).
[13]A. Ashkin, "Optical trapping and manipulation of neutral particles using lasers," Proc. Natl. Acad. Sci. **94**, 4853 (1997).
[14]L. Novotny, R. X. Bian, and X. S. Xie, "Theory of nanometric optical tweezers," Phys. Rev. Lett. **79**, 645 (1997).
[15]D. G. Kotsifaki and S. Nic Chormaic, "Plasmonic optical tweezers based on nanostructures: Fundamentals, advances and prospects," Nanophotonics **8**, 1227 (2019).
[16]M. Daly, M. Sergides, and S. Nic Chormaic, "Optical trapping and manipulation of micrometer and submicrometer particles," Laser Photonics Rev. **9**, 309 (2015).
[17]A. A. Al Balushi, A. Kotnala, S. Wheaton, R. M. Gelfand, Y. Rajashekara, and R. Gordon, "Label-free free-solution nanoaperture optical tweezers for single molecule protein studies," Analyst **140**, 4760 (2015).
[18]X. Han, V. G. Truong, P. S. Thomas, and S. Nic Chormaic, "Sequential trapping of single nanoparticles using a gold plasmonic nanohole array," Photonics Res. **6**, 981 (2018).
[19]D. G. Kotsifaki, M. Makropoulou, and A. A. Serafetinides, "Efficient and low cost multiple optical trap, based on interference," Optik **124**, 617 (2013).
[20]B. J. Roxworthy, K. D. Ko, A. Kumar, K. H. Fung, E. K. C. Chow, G. L. Liu, N. X. Fang, and K. C. Toussaint, "Application of plasmonic bowtie nanoantenna arrays for optical trapping, stacking, and sorting," Nano Lett. **12**, 796 (2012).
[21]X. Han, V. G. Truong, and S. Nic Chormaic, "Efficient microparticle trapping with plasmonic annular apertures arrays," Nano Futures **2**, 035007 (2018).
[22]T. D. Bouloumis, D. G. Kotsifaki, X. Han, S. Nic Chormaic, and V. G. Truong, "Fast and efficient nanoparticle trapping using plasmonic connected nanoring apertures," Nanotechnology **32**, 025507 (2021).
[23]M. Sergides, V. G. Truong, and S. Nic Chormaic, "Highly tunable plasmonic nanoring arrays for nanoparticle manipulation and detection," Nanotechnology **27**, 365301 (2016).
[24]E. Jaquay, L. J. Martínez, C. A. Mejia, and M. L. Povinelli, "Light-assisted, templated self-assembly using a photonic-crystal slab," Nano Lett. **13**, 2290 (2013).
[25]E. Jaquay, L. J. Martínez, N. Huang, C. A. Mejia, D. Sarkar, and M. L. Povinelli, "Light-assisted, templated self-assembly of gold nanoparticle chains," Nano Lett. **14**, 5184 (2014).
[26]B. A. Kemp, "Resolution of the Abraham-Minkowski debate: Implications for the electromagnetic wave theory of light in matter," J. Appl. Phys. **109**, 111101 (2011).
[27]D. G. Kotsifaki, M. Makropoulou, and A. A. Searfetinides, "Nanometric plasmonic optical trapping on gold nanostructures," Eur. Phys. J. Appl. Phys. **86**, 30501 (2019).
[28]V. A. Fedotov, N. Papasimakis, E. Plum, A. Bitzer, M. Walther, P. Kuo, D. P. Tsai, and N. I. Zheludev, "Spectral collapse in ensembles of metamolecules," Phys. Rev. Lett. **104**, 223901 (2010).
[29]E. Plum, K. Tanaka, W. T. Chen, V. A. Fedotov, D. P. Tsai, and N. I. Zheludev, "A combinatorial approach to metamaterials discovery," J. Opt. **13**, 055102 (2011).
[30]A. Kotnala and R. Gordon, "Quantification of high-efficiency trapping of nanoparticles in a double nanohole optical tweezer," Nano Lett. **14**, 853 (2014).
[31]Z. Xu, W. Song, and K. B. Crozier, "Direct particle tracking observation and Brownian dynamics simulations of a single nanoparticle optically trapped by a plasmonic nanoaperture," ACS Photonics **5**, 2850 (2018).
[32]G. Baffou, C. Girard, and R. Quidant, "Mapping heat origin in plasmonic structures," Phys. Rev. Lett. **104**, 136805 (2010).
[33]M. L. Brongersma, N. J. Halas, and P. Nordlander, "Plasmon-induced hot carrier science and technology," Nat. Nanotechnol. **10**, 25 (2015).
[34]J. C. Ndukaife, A. V. Kildishev, A. G. A. Nnanna, V. M. Shalaev, S. T. Wereley, and A. Boltasseva, "Long-range and rapid transport of individual nano-objects by a hybrid electrothermoplasmonic nanotweezer," Nat. Nanotechnol. **11**, 53 (2016).
[35]B. J. Roxworthy, A. M. Bhuiya, S. P. Vanka, and K. C. Toussaint, "Understanding and controlling plasmon-induced convection," Nat. Commun. **5**, 3173 (2014).
[36]A. Kotnala, P. S. Kollipara, J. Li, and Y. Zheng, "Overcoming diffusion-limited trapping in nanoaperture tweezers using opto-thermal-induced flow," Nano Lett. **20**, 768 (2020).